Photoresponsive halogen-bonded liquid crystals: The role of aromatic fluorine substitution

Marco Saccone,[1] Matthias Spengler,[1] Michael Pfletscher,[1] Kim Kuntze,[2] Matti Virkki,[2] Christoph Wölper,[3] Robert Gehrke,[1] Georg Jansen,[1] Pierangelo Metrangolo,[4] Arri Priimagi,[2*] and Michael Giese[1*]

1 Institut für Organische Chemie, Universität Duisburg-Essen, Universitätsstr. 7, 45141 Essen, Germany and CENIDE.

2 Laboratory of Chemistry and Bioengineering, Tampere University of Technology, P.O. Box 541, FI-33101 Tampere, Finland.

3 Institut für Anorganische Chemie, Universität Duisburg-Essen, Universitätsstr. 7, 45141 Essen, Germany.

4 Dipartimento di Chimica, Materiali e Ingegneria Chimica "Giulio Natta", Politecnico di Milano, Via Mancinelli 7, 20131, Milano, Italy.

KEYWORDS. halogen bonding, liquid crystals, photoresponsive materials, supramolecular chemistry

ABSTRACT: A new strategy for controlling the liquid crystalline and photo-physical properties of supramolecular mesogens assembled via halogen bonding is reported. Changing the degree of fluorination at the halogen-bond donor of the supramolecular liquid crystal allows for the fine tuning of the halogen bond strength and thereby provides control over the temperature range of the mesophase. At least three fluorine atoms have to be present in order to ensure efficient polarization of the halogen bond donor and the formation of a mesophase. In addition, it was found that stilbazole acceptors are superior to their azopyridine counterparts in promoting stable LC phases. The halogen-bond driven supramolecular liquid crystals between fluorinated azobenzenes and stilbazole/azopyridine acceptors show a rich variety of photoinduced processes driven by azobenzene photoisomerization, dictated not only by the photochemical properties of the molecular components, but also by the difference between the operation temperature and the clearing point.

Introduction

Within the past decades supramolecular chemistry has developed into an efficient tool for the design and synthesis of functional materials such as responsive polymers,[1] gels[2] and liquid crystals.[3] The employment of non-covalent bonds provides many advantages such as facile synthesis by self-assembly of pre-tailored building blocks or dynamic response to external stimuli or damages (self-healing/-repair).[1] The different intermolecular interactions, which have their specific characteristics (e.g. directionality or selectivity) and vary dramatically in their strengths, providing inexhaustible opportunities to create functional and responsive materials.

Recently, yet another interaction has been introduced into the toolbox of supramolecular chemistry – the halogen bond.[4] Halogen bonding takes place between a polarized halogen atom (the halogen-bond donor) acting as electron acceptor and an electron donor (halogen-bond acceptor) such as amine or pyridine.[5] The benefits of halogen bonding as compared to other non-covalent interactions are its high directionality and tunability.[6] These properties render halogen bonding particularly attractive for the design of supramolecular liquid crystals (LCs). The first halogen-bonded LCs were reported by Bruce and coworkers,[7] after which the field has grown substantially, and several different halogen-bond donating species such as iodoperfluoroalkanes,[8] iodoacetylenes,[9] and molecular iodine,[10] have been used.

The incorporation of light-responsive units such as azobenzenes into liquid crystals is an attractive approach for gaining external control over the alignment of the mesogens by using a non-invasive stimulus. Light-responsive LCs and LC polymers bear huge potential for tunable photonics and photomechanics,[11–13] and at more fundamental level, for photo-controlled self-assembly processes with light.[14,15] Azobenzenes are particularly interesting in this context because of their large and reversible shape change upon *trans-cis* photoisomerization and the incompatibility of the bent *cis*-azobenzene configuration with calamitic mesophases.[11] To obtain bistable photoswitching, *ortho*-fluorinated azobenzenes are particularly promising and their *cis*-lifetimes can range even up to several years.[16] An additional bonus of fluorination is that it allows to tailor the anisotropy and viscoelastic properties of LCs, which has been utilized in devising self-assembled structures with ever-increasing complexity and, from a more practical perspective, state-of-the-art liquid-crystal displays.[17]

Ortho-fluorinated azobenzenes with long *cis*-isomer lifetimes were recently used by us to produce halogen-bonded LCs with a variety of photochemical phase transitions.[18] We tuned the thermal properties of the LC assemblies by varying the length of the pendant chains of the aromatic building blocks. Already earlier, our results[19] as well as the results of others[20,21] have highlighted the fact that halogen bonding is a highly attractive supramolecular tool for devising photo-responsive materials.[22] Although a number of theoretical studies suggest the tunability of the halogen bond by changing the fluorine substitution pattern at the halogen-bond donor, this approach has not been used in materials applications so far.[23]

In the present study, we comprehensively investigate the impact of the halogen bond strength on the phase behavior of supramolecular liquid crystals. The strength of the halogen bond is systematically tuned from two sides: (i) the donor (**D**) side by varia-

tion of the fluorine substitution pattern, which influences the halogen-bond donating capability as well as the photochemical properties of the assemblies, and (ii) the acceptor (**A**) side, by comparing azo- and ethylene-linkers (**Scheme 1**). Our study contributes to the future design of halogen-bond based supramolecular LCs and systematic improvement of their thermal and photoresponsive properties.

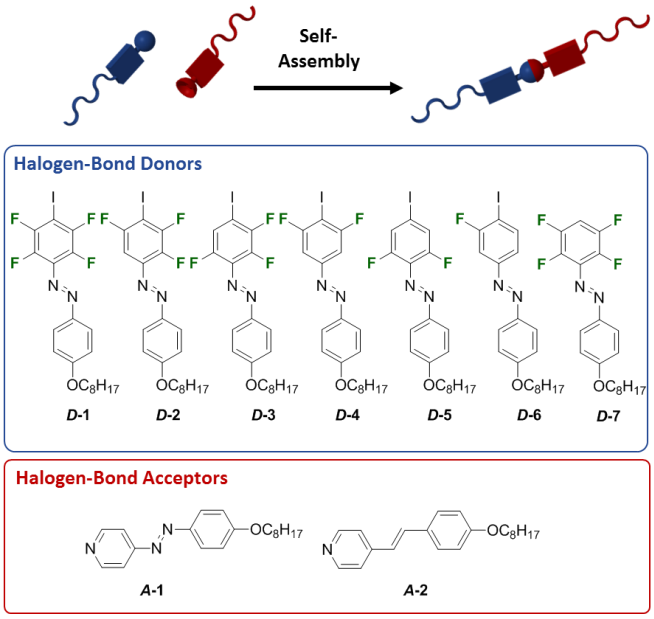

Scheme 1. Modular approach to investigate the impact of the strength of the halogen bond on the liquid crystalline behavior of the supramolecular assemblies.

Results and Discussion

Materials Design

It is well known that reducing the number of fluorine atoms at the halogen-bond donating arene weakens the strength of the halogen bond.[23b] In addition, the fluorine substitution pattern at the arene provides control over the photochemical properties of the halogen-bond donating azobenzenes.[16b,24] The properties of supramolecular assemblies strongly depend on the interplay between the intermolecular forces present in the system, and it is essential to elaborate, to the extent possible, the individual contributions of the interactions involved for the design of high-performance supramolecular materials. Herein, we investigate the impact of the fluorination pattern on the properties of halogen-bonded liquid crystals by preparation of a series of dimeric complexes between halogen-bond donors with different fluorination patterns within the ring (***D***-1 – ***D***-6) and 4-alkoxyazopyridines (***A***-1) or 4-alkoxystilbazoles (***A***-2) as halogen-bond acceptors (Scheme 1). As in our previous investigations,[18] we used halogen-bond donating azobenzenes motivated by the fact that the fluorine substitution pattern at the arene provides control over the photochemical properties of the molecules. The rationale behind the choice of ***A***-1 and ***A***-2 lies in the observation that both are effective promesogenic molecules which have been used successfully in the design of halogen-bond based LCs.[7,20]

Theoretical Insights

We first studied the azobenzene XB donors ***D***-1 – ***D***-6 and their complexes with ***A***-1 and ***A***-2 using dispersion-corrected density functional theory (DFT+D), replacing the alkoxy groups with hydroxy groups for computational efficiency. Computational analysis is highly pertinent since subtle variations of the structure of the halogen-bond donor are known to have a huge impact on the formation of LC phases. For example, Bruce *et al.* reported that iodopentafluorobenzene forms liquid crystalline assemblies with stilbazoles, while bromopentafluorobenzene does not.[7] Another example was reported by Yu and coworkers, who obtained halogen-bonded LC complexes by combination of azopyridine with molecular iodine and bromine, whereby the complexes with broadest LC temperature ranges employed molecular bromine, not iodine (even if the latter yields stronger halogen bonding).[20]

In a simplified view, the nature of halogen bonds can be described as mainly electrostatic.[5b] Therefore, we computed the molecular electrostatic potentials of the halogen-bond acceptors and donors to understand their capabilities to form halogen-bond complexes. Looking at the electrostatic surface potentials of the XB acceptors (Figure S5), it can be seen that ***A***-1 shows a minimum value on the nitrogen atom (-183.8 kJ/mol) that is more positive compared to that in the stilbazole ***A***-2 (-190.5 kJ/mol), indicating that the latter is a stronger halogen-bond acceptor than the azopyridine.

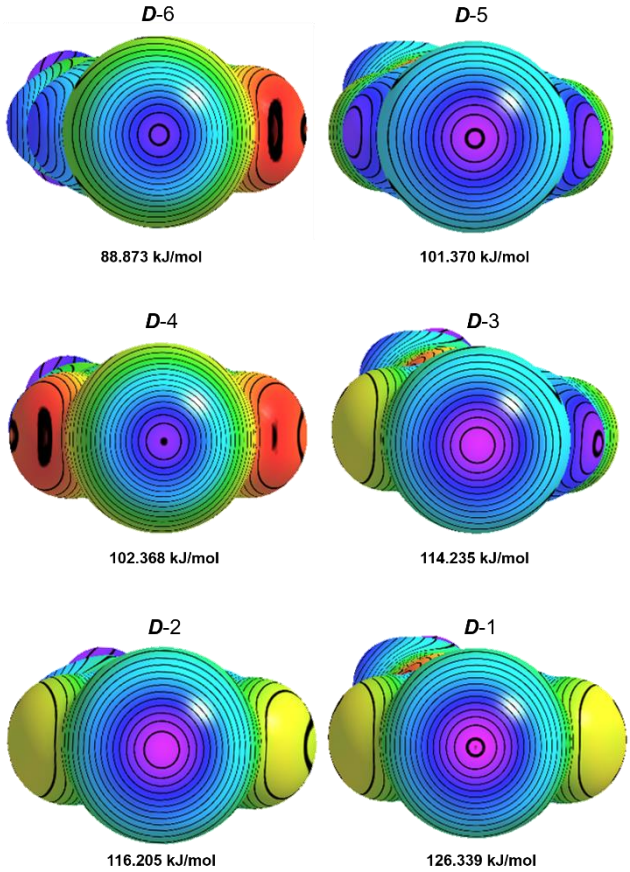

Figure 1. Molecular electrostatic potentials of ***D***-1 – ***D***-6 plotted on the 0.001 au contour of the electron density. The electrostatic potential on the iodine atom increases (more positive) as the number of fluorine atoms is increased. Color gradient: from deep red (most negative), to violet (most positive)

The electrostatic potentials of the halogen-bond donors are shown in **Figure 1** (see also Figure S7). The evolution of the iodine potential and its dependence on the fluorination degree and substitution pattern is clearly visible. The electrostatic potential has the maximum (most positive) value on the iodine atom at the tetrafluorinated ring (***D***-1) and decreases systematically with decreasing number of fluorine atoms on the aromatic ring as reported in Figure 1. Hence, as expected, higher fluorination degree at the aromatic core strengthens the halogen bond. Also the substitution pattern at the arene plays a role and has an impact on the polariza-

tion of the iodine atom. ***D***-2 and ***D***-3 both bear three fluorine atoms at the halogen-bond donating arene ring. However, in ***D***-2 the iodine atom is paneled by two fluorine atoms leading to a slightly stronger polarization when compared to ***D***-3, where only one fluorine atom is in close proximity to the iodine. Finally, we computed the interaction energies for all the assemblies (**Figure 2**, Table S1) and found their magnitudes to decrease in the order ***D***-1·***A***-2 > ***D***-2·***A***-2 > ***D***-3·***A***-2, with the stilbazole assemblies always being more stabilized compared to the azopyridine assemblies (*i.e.* ***D***-1·***A***-2 > ***D***-1·***A***-1; ***D***-2·***A***-2 > ***D***-2·***A***-1 and so on).

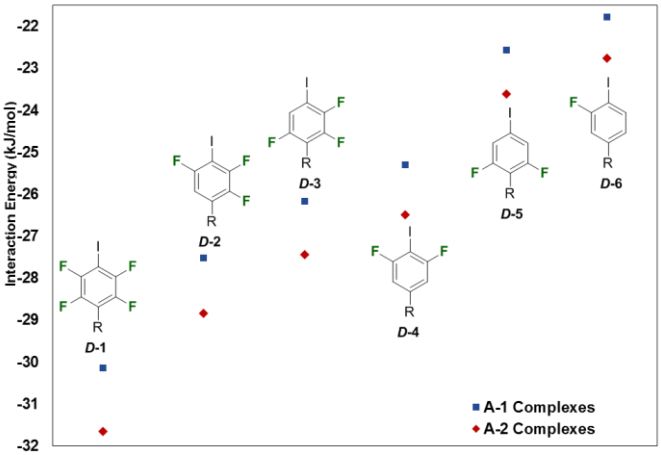

Figure 2. Graphical representation of the interaction energies of the halogen-bonded complexes.

Crystallographic Analysis

In total, 12 halogen-bonded complexes were obtained by self-assembly of ***D*** and ***A*** by slow room-temperature evaporation of acetonitrile solutions. With the aim of elucidating the supramolecular organization of the starting materials in the co-crystals, we were able to obtain crystal structures of ***D***-1, ***D***-2 and ***D***-3 with short-alkyl-chain stilbazoles (***St***-n, where n is the length of the alkoxy chain). The choice of keeping the alkoxy chain short, instead of directly using ***A***-2, was dictated by the fact that for ***A***-2 complexes, no crystal structures could be obtained. Our structures are closely related to those reported by Fernandez-Palacio *et al.*[18a] using ***D***-1, however, the following discussion will focus on findings relevant for the present investigation.

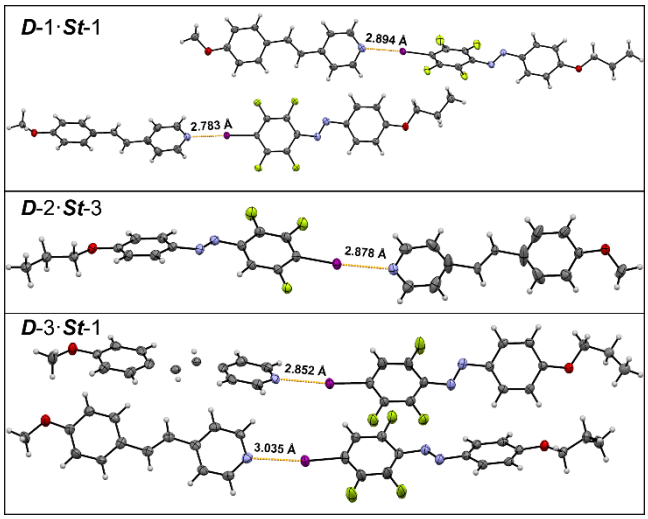

Figure 3. ORTEP representation of the halogen-bonded co-crystals ***D***-1·***St***-1, ***D***-2·***St***-3, and ***D***-3·***St***-1. Color code: gray, C; white, H; red, O; blue, N; yellow, F; and magenta, I. Halogen bonds are represented by orange dotted lines. Ellipsoids are drawn at 50% probability and disordered fragments are omitted for clarity.

D-1 – ***D***-3 and ***St***-n are assembled into supramolecular dimers by short and highly directional I···N(pyr) halogen bonds (**Figure 3**). The respective I···N distances and C–I···N angles are given as follows: 2.783(2) Å, 173.55° and 2.894(2), 175.25° in ***D***-1·***St***-1; 2.878(1) Å and 174.85° in ***D***-2·***St***-3; 2.852(2) Å, 173.3° and 3.055(2), 171.8° in ***D***-3·***St***-1. The observed halogen-bond distances roughly correspond to 25% (in the case of the shortest halogen bond involving ***D***-1·***St***-1) and 17% (in the case of the longest halogen bond involving ***D***-3·***St***-1) reduction of the sum of the van der Waals radii of I and N, respectively.[25] At variance with what it was reported by Fernandez-Palacio *et al*., arene-perfluoroarene interactions were found to have no role in the packing of the present structures. An interesting feature is that in the structures reported the aromatic rings in the azobenzenes are not coplanar, instead a certain degree of twist between them is present. We believe this to be due to partial fluorination of such rings that lead to a strong steric repulsion between the fluorine atoms and the neighboring azo group[26] We started our analysis with geometrical descriptors only, in a "the shorter, the stronger" perspective,[27] being perfectly aware that this view of chemical bonding (thus including the halogen bond) has been recently criticized because, in most cases, it lacks of computational support.[28] Under this perspective a tentative trend of effectiveness in halogen-bond formation is given by ***D***-1 > ***D***-2 > ***D***-3, *i.e.* the perfluoroiodo synthon is stronger than the two trifluoroiodo synthons where the *meta*-difluorinated ***D***-2 (*meta* to the azo) prevails over ***D***-3. This is in agreement with our DFT calculations, showing that a simplistic "the shorter, the stronger" view of halogen-bonding interaction seems computationally justified in our case.

Mesomorphic Behavior

The complexes were analyzed using polarized optical microscopy (POM) and differential scanning calorimetry (DSC) and exclusively showed nematic phases. In general, we observed good agreement among POM and DSC data, except for ***D***-2-***A***-1, for which no indication for the Iso→N transition was found by DSC. We attribute this to the small temperature range of the nematic phase, the transition being overshadowed with the N→Cr transition. None of the building blocks showed liquid crystalline behavior by themselves, and, in order to exclude an induction of liquid crystallinity exclusively by π-π-interactions, the non-iodinated analogue ***D***-7 was prepared as a reference. The respective combinations with ***A***-1 and ***A***-2 did not show any mesomorphism.

Some representative POM pictures of the thermotropic LC phases are shown in **Figure 4** and Figures S7 and S8. The DSC data is given in the supporting information (Tables S3 and S5), while a chart with the phase transitions as determined by POM is given in **Figure 5**.

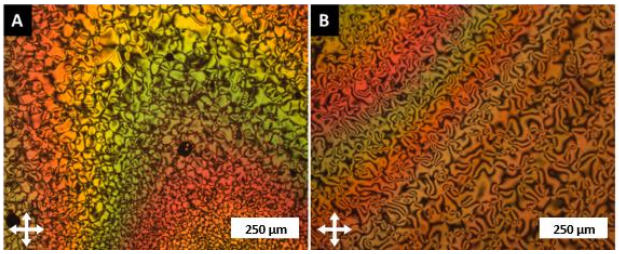

Figure 4. POM pictures of the unaligned N phase as observed for the ***D***-1·***A***-1 at 96 °C (A) and ***D***-1·***A***-2 at 110 °C (B).

As mentioned earlier, the properties of supramolecular materials are the result of a complex interplay of various non-covalent interactions, which makes unambiguous structure-property correla-

tions challenging. Changing the fluorination degree of the halogen-bond donor reduces its capability to form halogen bonds. At the same time the electronic nature of the π-systems and the dielectric anisotropy of the whole assembly is affected. However, the following discussion focuses, in a simplified view, on the halogen bonds and correlates their strengths with the thermal behavior of the assemblies. The results indicate a strong impact of the halogen-bond tuning on the thermal behavior of the halogen bond assemblies. The nature of the halogen-bond acceptor ***A*** as well as the substitution pattern of the iodinated halogen-bond donor ***D*** influences the phase transition temperatures and the mesomorphic properties of the complexes.

Impact of the Halogen-Bond Acceptor. The complexes prepared by mixing the halogen-bond donors ***D*** with the azopyridine ***A***-1 invariably displayed lower thermal stability compared to their stilbazole analogues formed with ***A***-2. Of the azopyridine complexes, only ***D***-1·***A***-1 showed an enantiotropic nematic phase with a temperature range of 9 °C (heating) or 13 °C (cooling). In addition, a monotropic nematic phase was observed for ***D***-2·***A***-1 with a temperature range of 5 °C. In contrast, three of the stilbazole complexes exhibited enantiotropic mesomorphism with an enhanced phase stability. We attribute the difference in the mesophase stability to (i) the lower halogen-bond accepting capability of the azopyridine, due to the electron-withdrawing effect of the azo-group,[29] and (ii) the repulsion of the free-electron pairs located at the azo-linkage that may have a negative effect on the mesophase stability.[30] The computation of the electrostatic potential of ***A***-1 shows a minimum value on the nitrogen atom which is more positive compared to the one in the stilbazole ***A***-2 indicating that the latter is a stronger XB acceptor than the azopyridine (Figure S5). This is also proven by the computed interaction energies of the assemblies (Figure 2 and Table S1), which are lower (less negative) for the azopyridines than for the stilbazole assemblies. As an example, the complex ***D***-1·***A***-1 shows an interaction energy of -30.15 kJ/mol, compared with -31.65 kJ/mol for ***D***-1·***A***-2, making the latter slightly more favorable.

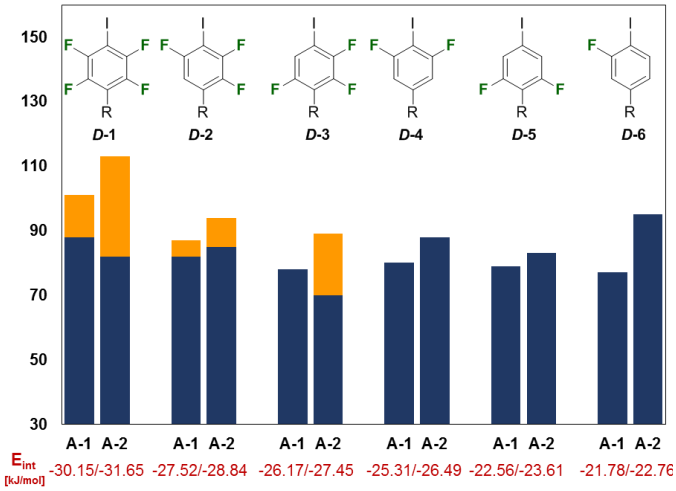

Figure 5. Chart of the thermal behavior of the studied complexes as determined by POM (cooling rate: 5 °C/min; blue: crystalline phase, yellow: nematic phase). The interaction energies for the complexes are given in kJ/mol (red numbers).

Impact of the Halogen-Bond Donor. The substitution pattern at the iodinated ring also has a strong effect on the properties of the assemblies. The following discussion will focus on the stilbazole-based complexes with the various halogen-bond donors as they outperform the corresponding azopyridine-based complexes in terms of LC phase formation and stability. Tetra- and trifluorinated halogen-bond donors ***D***-1·***A***-2 (ΔT = 31 °C on cooling), ***D***-2·***A***-2 (ΔT = 9 °C on cooling) and ***D***-3·***A***-2 (ΔT = 19 °C on cooling) exhibited nematic mesophases as shown by POM and DSC (Figure S8), while the di- or mono-fluorinated halogen-bond donors did not show any mesomorphic behavior. In contrast to the calculated interaction energies of the assemblies, which show a stronger interaction in ***D***-2·***A***-2 (E_{int} = -28.84 kJ/mol) than in ***D***-3·***A***-2 (E_{int} = -27.45 kJ/mol; see Table S1 in the supporting information), ***D***-3·***A***-2 showed a broader mesophase range than ***D***-2·***A***-2 upon cooling. This difference may be due to suppression of the crystallization by the tilting of the **D**-3 moiety due to the fluorination in *ortho*-position to the azo-group.[31] These results show that at least three fluorine atoms are needed at the halogen-bond donor moiety to obtain sufficiently strong halogen bonding for the stabilization of the mesophase, indicating that subtle changes in the interaction energies have a significant impact on the properties of the supramolecular assemblies.

Photoresponsive Behavior

As mentioned earlier, the azobenzene fluorination pattern not only affects the capability to act as halogen-bond donor, but also the photochemical properties, particularly *cis*-lifetimes. Therefore, we characterized the compounds ***D***-1 – ***D***-7 in solution in terms of their photoresponsivity prior to studying the halogen-bond driven LC phases. **Table 1** shows the absorption maxima as well as the thermal half-lives of the *cis*-isomers of the compounds in a 10^{-5} M DMF solution upon irradiation with a wavelength of 365 nm (intensity ca. 100 mW cm^{-2}). Further details on the *cis*-lifetime determination, as well as absorption spectra for all molecules in the all-*trans* and photostationary states, are given in the supporting information (Figures S9 and S10). As expected based on the findings of Bléger *et al.*,[16b] the lifetimes of the *ortho*-difluorinated XB donors are roughly one order of magnitude longer than those which do not feature this fluorination pattern. Interestingly, among the three *ortho*-difluorinated XB donors, ***D***-1, ***D***-3, and ***D***-5, the *cis*-lifetime systematically increases with *decreasing* number of fluorine atoms, i.e., ***D***-5 > ***D***-3 > ***D***-1, being 43 days for the former. This highlights that both steric and subtle electronic effects are important in determining the *cis*-lifetimes, as also confirmed by comparing ***D***-1 with its non-iodinated analogue ***D***-7. The latter exhibits a 3.5-fold increase in the *cis*-lifetime. By comparing the molecular electrostatic potentials (Figure 1), the halogen-bond interaction strengths (Figure 2) and the *cis*-lifetimes of ***D***-1, ***D***-3, and ***D***-5, an inverse relationship can be observed: the molecule yielding the longest *cis*-lifetime (***D***-5) exhibits the weakest halogen bond with both ***A***-1 and ***A***-2, and the complexes are not liquid-crystalline. As a comparison, in complexes between azophenols and stilbazoles, driven by strong phenol-pyridine hydrogen bonding, *ortho*-difluorination markedly stabilizes the LC phase.[32] An interesting future prospect is also to extend the study on fluorinated photoresponsive LCs towards bond donors with *ortho*-tetrafluorination as a means to further increase the *cis*-lifetime.[16]

Table 1. The *cis-trans* thermal half-lifes and π–π* absorption maxima for the XB donor molecules as determined in dilute DMF solution at 25 °C.

Molecule	***D***-1	***D***-2	***D***-3	***D***-4	***D***-5	***D***-6	***D***-7
$\tau_{1/2}$ (days)	12	1.7	19	2	43	1.7	40.1
λ_{max} (nm)	364	359	372	367	348	365	355

As for photoresponsivity in the LC state, this study is a follow-up to our previous work on ***D***-1·***A***-2,[18a] targeting towards elaborating (i) the role of the halogen-bond acceptor (azopyridine *versus* stilbazole), and (ii) the strength of the halogen-bond donor (***D***-1

vs. ***D***-2 *vs*. ***D***-3) on the photoinduced phase transitions. Herein we summarize our main observations.

The comparison between the two XB acceptors, ***A***-1 and ***A***-2, was conducted using the donor that resulted in most stable LC phases, ***D***-1. The main difference between the acceptors is that ***A***-1 itself is photoresponsive (Figure S10) and has a *cis*-lifetime of 3.8 h at room temperature in a dilute DMF solution, while ***A***-2 is not photoactive under the experimental conditions used. However, ***A***-2 systematically yields stronger halogen bonds with the XB donors (Figure 2), as well as more stable LC phases (Figure 5). We first irradiated the samples in the liquid-crystalline state with 405 nm light (30 s, 40 mW/cm^2) and monitored the photoinduced transition to the isotropic state and reorganization of the LC phase via birefringence and optical scattering measurements in planar LC cells with 2 µm thickness. The experimental temperatures of 94 °C for ***D***-1·***A***-1 and 96 °C ***D***-1·***A***-2 were chosen, since they lie as close as possible to each other yet yield stable mesophases without crystallization of the sample during the experimental time frame. The most important finding is that the recovery of the LC phase for ***D***-1·***A***-1 with its two photoisomerizable components takes significantly longer than for ***D***-1·***A***-2 (890 s compared to 250 s), where only ***D***-1 is activated (we confirmed that stilbazole does not isomerize upon 405 nm irradiation). This is clearly evident from **Figure 6a**: Photoinduced LC-to-isotropic transition leads to a rapid loss of birefringence (Δ*n*) of both samples, accompanied by a strong transient peak in optical scattering (Attenuance, Att.) due to photoinduced phase separation into *trans*-rich and *cis*-rich domains.[33] The lifetime of the isotropic state is associated with the recovery of the birefringence and the simultaneous increase in optical scattering, due to recovery of the LC phase induced by thermal *cis–trans* isomerization.

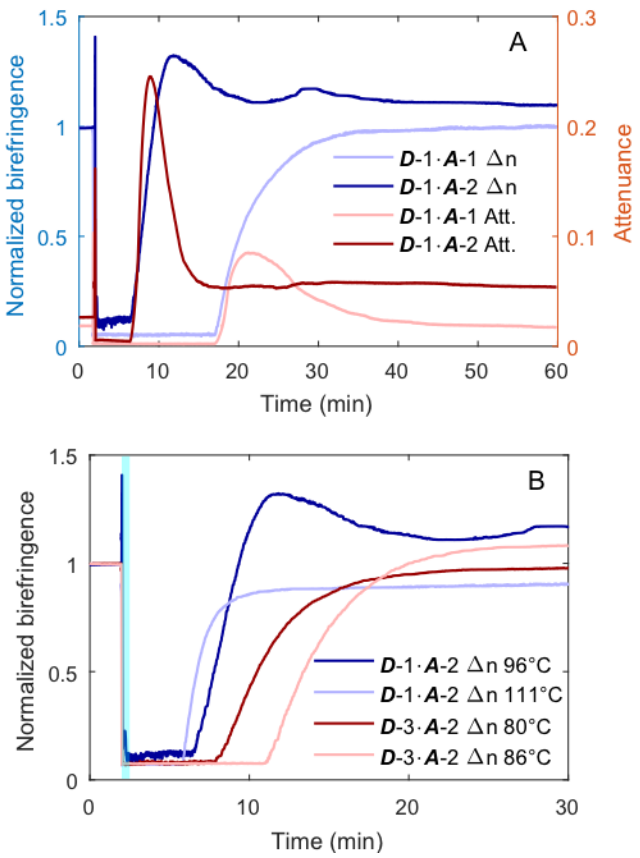

Figure 6. a) Normalized birefringence (Δn) at 676 nm and attenuance (Att.) at 635 nm for ***D***-1·***A***-1 at 94 °C and ***D***-1·***A***-2 at 96 °C. b) Normalized birefringence for ***D***-1·***A***-2 at 96 and 111 °C, and for ***D***-3·***A***-2 at 80 and 86 °C.

Having photoisomerizable moieties in both donor and acceptor prolonging the relaxation time, seems intuitive by hindsight. However, we note that the *cis*-lifetimes of ***D***-1 and ***A***-1 at 94 °C are 545 s and 16.2 s, respectively, and their absorption maxima are comparable (364 nm and 357 nm, respectively). Therefore, the differences in the recovery times are not connected to the use of a photoresponsive acceptor, but instead to the different stabilities of the LC phases at 94 °C (***D***-1·***A***-1) and 96°C (***D***-1·***A***-2), respectively. Whereas ***D***-1·***A***-1 is close to the transition to the isotropic phase, ***D***-1·***A***-2 lies near its crystallization temperature, causing the LC phase of the latter to be more stable. This may allow for the presence of a higher fraction of *cis*-isomer while still retaining the LC phase. To test this assumption, we repeated the experiment for ***D***-1·***A***-2 at 111 °C, close to the upper limit of its LC range. At this temperature the lifetime of the isotropic state is only slightly shorter than at 96 °C (200 s *vs*. 250 s; Figure 6b), even if the *cis*-lifetime is significantly decreased due to the temperature increase. Comparing the isotropic state lifetimes close to the clearing point, *i.e.*, ***D***-1·***A***-1 at 94 °C (890 s) and ***D***-1·***A***-2 at 111 °C (200 s), on the other hand, seems directly dictated by the *cis*-lifetime differences between the donors at these temperatures (545 s and 128 s, respectively). Therefore, we can conclude that while *cis*-lifetime is indeed important in dictating the stability of the photoinduced isotropic state, direct comparison between photoresponsive units can only be conducted at equal point in the phase diagram, e.g. close to the clearing point.

The comparison between ***D***-1 – ***D***-3, conducted only using ***A***-2, provided results qualitatively similar to our earlier studies on ***D***-1·***A***-2.[18a] The experiments were again performed in 2 µm planar LC cells, and the photoinduced isotropization was studied at two temperatures for each sample, with the first one being close to the crystallization temperature (96 °C and 80 °C for ***D***-1·***A***-2 and ***D***-3·***A***-2, respectively) and the second one being close to the clearing point (111 °C and 86 °C, respectively). Note that the nematic phase of ***D***-2·***A***-2 spontaneously crystallized within a few minutes, making direct comparison with ***D***-1·***A***-2 and ***D***-3·***A***-2 impossible. However, fast and reversible crystal-to-isotropic transition was observed for this complex, as illustrated in **Figure 7**. As already discussed, the recovery of the N phase took 250 and 200 s for ***D***-1·***A***-2 at 96 and 111 °C, respectively. For ***D***-3·***A***-2, the photoinduced isotropic state lifetime was 330 s at 80 °C and 540 s at 86 °C (Figure 6b), *i.e.*, significantly shorter at lower temperature where the *cis*-lifetime is longer. This unintuitive result clearly highlights that even more than the *cis*-lifetime, the difference between the measurement temperature and the clearing point is a key parameter when analyzing photoinduced phase transitions and their thermal stability in (supramolecular) LCs.

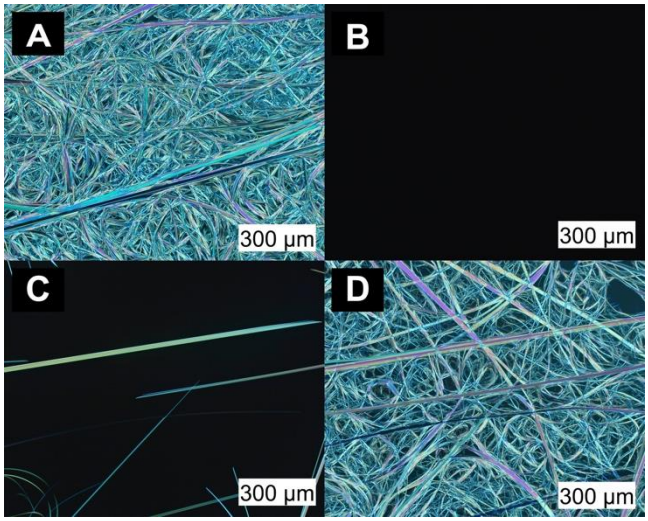

Figure 7. POM images of ***D***-2·***A***-2 at 93 °C a) before irradiation, b) immediately after irradiation with 405 nm light (30 s, 40 mW cm^{-2}), c) 3 min, and d) 5 min after ceasing the irradiation.

Conclusions

We have demonstrated that supramolecular halogen-bonded liquid crystals can be systematically achieved by fine tuning the halogen bond strength by changing the degree of fluorination at the halogen-bond donor. Our results show that at least three fluorine atoms need to be present in order to form stable LC assemblies, while adducts with a lower fluorination degree do not exhibit any LC properties. We thus established a hierarchy among different halogen-bond donors in driving the LC phase formation as it has been done in crystal engineering[34a] and photoresponsive polymers[34b]. We also found the stilbazoles to form more stable mesophases compared to azopyridines. The resulting halogen-bond driven supramolecular liquid crystals between azobenzene and stilbazole molecules exhibit a rich variety of photoinduced processes, including photoinduced LC-to-isotropic phase transitions whose stability is not only dictated by the photochemical properties of the molecular components, but also by the difference between the measurement temperature and the clearing point. To draw some design guidelines for stabilizing the photoinduced isotropic state, we therefore propose to use donors/acceptors with long-lived metastable states and LC phases that not only occur close to room temperature but also exhibit low clearing points.

Experimental Section

Methods

All commercially available compounds and solvents were used without further purification as received from suppliers. ^{1}H-, ^{19}F-, and ^{13}C-NMR-Spectra of the compounds were collected in deuterated solvents ($CDCl_3$, DMSO) at room temperature if not otherwise stated using a *Bruker* DMX 300 or a *Bruker* DRX 500 (600 MHz). Mass spectra were obtained with a *Bruker* amazon SL (LRMS) or a MaXis 4G Q-TOF-mass spectrometer (HRMS). IR-spectra were recorded with a *Jasco* FT/IR-430 Spectrometer. DSC data were collected using a DSC 3+/700/866/Argon from *Mettler Toledo* equipped with an intra cooler. The samples were measured in 40 µL standard almunium crucibles with a heating and cooling rate of 5 K/min. Polarized optical microscopy (POM) images/videos were taken on a *Nikon* Eclipse Ni microscope equipped with crossed polarizers, a *Linkam* LinkPad hot stage, and an *OptixCam Summit* K2 OCS-D3K4-14 microscope camera. *Cis*-lifetimes in solution were measured using an *Agilent* Cary 60 spectrophotometer and a large custom-built cavity with an *Ocean Optics* qpod 2e temperature-controlled cuvette holder and a *Prior Scientific* Lumen-1600 light source. The light-responsive properties of the ILCs were studied using an *Avantes* AvaSpec-2048L fiber-optic spectrometer and an *Avantes* AvaLight-DH-S-BAL balanced deuterium-halogen light source coupled to a vertical-beam custom cavity equipped with a *Linkam* LinkPad temperature controller and a *Thorlabs* M405FP1 photoexcitation light source. The birefringence was simultaneously studied using a second, almost collinear beam line from a *Thorlabs* CPS670F (676 nm) laser with crossed polarizers before and after the sample and a *Thorlabs* PD100A-EC photodiode.

Synthetic Procedures

Alkoxystilbazoles, alkoxyazopyridines and ***D***-1 are known molecules, while the other fluorinated azobenzenes were prepared by a $NOBF_4$-mediated diazotization reaction between the appropriate fluoroaniline and phenol to produce first the azophenols, that were then alkylated with 1-bromooctane. Reactions were carried out in oven-dried glassware under a nitrogen atmosphere. Complete details about the synthesis are given in the supporting information, here the data for the molecules ***D***-2–***D***-6 are reported.

D-2**:** Yield 24%, m.p. 76 °C; ^{1}H NMR (600 MHz, DMSO d_6): δ = 7.95 – 7.90 (m, 2H), 7.44 – 7.38 (m, 1H), 7.17 – 7.12 (m, 2H), 4.12 (t, *J*=6.5, 2H), 1.80 – 1.73 (m, 2H), 1.49 – 1.41 (m, 2H), 1.39 – 1.18 (m, 10H), 0.88 (t, *J*=7.0, 3H); ^{13}C NMR (151 MHz, DMSO d_6): δ = 162.66 (s), 145.89 (s), 125.22 (s), 115.13 (s), 98.58 (dd, *J*=28.5, 3.3), 68.06 (s), 30.82 (s), 28.29 (s), 28.21 (s), 28.19 (s), 25.06 (s), 21.63 (s), 13.45 (s); ^{19}F NMR (565 MHz, DMSO d_6): δ= -98.31 (dd, *J*=12.6, 8.4, 1F), -115.30 (dd, *J*=23.3, 1.4, 1F), -151.87 (ddd, *J*=22.9, 12.8, 5.6, 1F). IR: n (cm^{-1}) = 3093, 3073, 2992, 2856, 1738, 1599, 1577, 1499, 1466, 1429, 1407, 1390, 1338, 1317, 1297, 1250, 1207, 1141, 1110, 1030, 999, 943, 898, 872, 838, 808, 758, 722, 679. MS (ESI): m/z (%): positive: 491.0807 (100, $[M+H]^+$, $[C_{20}H_{22}F_3IN_2O+H]^+$, calc.: m/z = 491.0802).

D-3**:** Yield 62 %, m.p. 56 °C; ^{1}H NMR (600 MHz, DMSO d_6): δ = 7.92 – 7.79 (m, 3H), 7.18 – 7.09 (m, 2H), 4.12 (t, *J*=6.5, 2H), 1.80 – 1.73 (m, 2H), 1.48 – 1.41 (m, 2H), 1.37 – 1.26 (m, 8H), 0.87 (t, *J*=6.9, 3H); ^{13}C NMR (151 MHz, DMSO d_6): δ= 162.66 (s), 146.70 (s), 124.73 (s), 120.86 – 120.76 (m), 120.62 (dd, *J*=24.1, 3.0), 115.07 (s), 68.06 (s), 30.82 (s), 28.24 (d, *J*=14.3), 25.05 (s), 21.63 (s), 13.44 (s); ^{19}F NMR (565 MHz, DMSO d_6): δ= -121.64 – -121.77 (m, 1F), -126.43 (dd, *J*=13.1, 10.1, 1F), -144.25 (dd, *J*=21.9, 1.9, 1F). IR: n (cm^{-1}) =3069, 2944, 2920, 2856, 1601, 1577, 1500, 1465, 1441, 1404, 1330, 1297, 1253, 1214, 1185, 1141, 1110, 1090, 1059, 1029, 1000, 968, 896, 850, 838, 810, 799, 759, 748, 723, 656.
MS (ESI): m/z (%): positive: 491.0800 (100, $[M+H]^+$, $[C_{20}H_{23}F_3IN_2O+H]^+$, calc.: m/z = 491.0802).

D-4: Yield 72%, m.p. 75 °C; ^{1}H NMR (500 MHz, DMSO d_6): δ = 7.87 – 7.79 (m, 2H), 7.75 – 7.67 (m, 2H), 7.15 – 7.08 (m, 2H), 4.11 (t, *J*=6.5, 2H), 1.80 – 1.72 (m, 2H), 1.49 – 1.40 (m, 2H), 1.40 – 1.21 (m, 9H), 0.88 (t, *J*=7.0, 3H); ^{13}C NMR (126 MHz, DMSO d_6): δ = 162.30 (s), 154.10 (dd, *J*=261.1, 4.9), 146.74 (s), 130.10 (t, *J*=10.4), 124.45 (s), 121.98 – 121.49 (m), 114.96 (s), 93.24 (t, *J*=7.9), 67.98 (s), 30.77 (s), 28.25 (s), 28.17 (s), 28.14 (s), 25.02 (s), 21.58 (s), 13.39 (s); ^{19}F NMR (471 MHz, DMSO d_6): δ= -121.64 (d, *J* = 8.7 Hz, 1F). IR: n (cm^{-1}) =3076, 2945, 2919, 2855, 1725, 1595, 1578, 1566, 1500, 1471, 1419, 1401, 1322, 1298, 12631201, 1140, 1109, 1049, 1000, 904, 839, 810, 800, 759, 723. MS (ESI): m/z (%): positive: 473. 898 (100, $[M+H]^+$, $[C_{20}H_{22}F_3IN_2O+H]^+$, calc.: m/z = 490.0896).

D-5: Yield 27 %, liquid; ^{1}H NMR (500 MHz, DMSO d_6): δ = 7.87 – 7.79 (m, 2H), 7.75 – 7.67 (m, 2H), 7.15 – 7.08 (m, 2H), 4.11 (t, *J*=6.5, 2H), 1.80 – 1.72 (m, 2H), 1.49 – 1.40 (m, 2H), 1.40 – 1.21 (m, 9H), 0.88 (t, *J*=7.0, 3H); ^{13}C NMR (126 MHz, DMSO d_6): δ = 162.30 (s), 154.10 (dd, *J*=261.1, 4.9), 146.74 (s), 130.10 (t, *J*=10.4), 124.45 (s), 121.98 – 121.49 (m), 114.96 (s), 93.24 (t, *J*=7.9), 67.98 (s), 30.77 (s), 28.25 (s), 28.17 (s), 28.14 (s), 25.02 (s), 21.58 (s), 13.39 (s); ^{19}F NMR (471 MHz, DMSO d_6): δ= -121.64 (d, *J* = 8.7 Hz, 1F). IR: n (cm^{-1}) =3076, 2945, 2919, 2855, 1725, 1595, 1578, 1566, 1500, 1471, 1419, 1401, 1322, 1298, 12631201, 1140, 1109, 1049, 1000, 904, 839, 810, 800, 759, 723. MS (ESI): m/z (%): positive: 473. 898 (100, $[M+H]^+$, $[C_{20}H_{22}F_3IN_2O+H]^+$, calc.: m/z = 490.0896).

D-6: Yield 64%, m.p. 63 °C; ^{1}H NMR (500 MHz, DMSO d_6): δ = 8.05 (dd, *J*=8.3, 6.9, 1H), 7.91 – 7.87 (m, 2H), 7.61 (dd, *J*=9.0, 2.1, 1H), 7.51 (dd, *J*=8.3, 2.1, 1H), 7.15 – 7.10 (m, 2H), 4.11 (t, *J*=6.5, 2H), 1.80 – 1.72 (m, 2H), 1.49 – 1.41 (m, 2H), 1.38 – 1.23 (m, 8H), 0.88 (t, *J*=6.9, 3H); ^{13}C NMR (126 MHz, DMSO d_6): δ = 161.88 (s), 161.51 (d, *J*=244.4), 153.57 (d, *J*=6.3), 145.66 (s), 139.61 (d, *J*=2.4), 124.59 (s), 120.46 (d, *J*=3.1), 114.93 (s), 107.44 (d, *J*=25.7), 84.06 (d, *J*=26.2), 67.93 (s), 30.77 (s), 28.25 (s), 28.20 (s), 28.15 (s), 25.03 (s), 21.58 (s), 13.39 (s); ^{19}F NMR (471 MHz, DMSO d_6): δ= -93.56 (dd, *J*=8.4, 7.4, 1F). IR: n (cm^{-1}) = 3069, 2944, 2918, 2852, 1603, 1582, 1501, 1469, 1398, 1318, 1296, 1259, 1234, 1145, 1130, 1106, 10433, 1024, 1000, 961, 925, 876, 840, 820, 754, 724, 694, 665. MS (ESI): m/z (%): positive: 455.0998 (100, $[M+H]^+$, $[C_{20}H_{24}FIN_2O+H]^+$, calc.: m/z = 455.0990).

Single-crystal X-ray analysis

The crystals were mounted on nylon loops in inert oil. Data were collected on a Bruker D8 Venture diffractometer with (Photon II detector) (mono-chromated $Cu_{K\alpha}$ radiation, λ = 1.54178 Å) at 100(2) K. The structures were solved by Direct Methods (SHELXS-97)[35] and refined anisotropically by full-matrix least-squares on F^2 (SHELXL-2014).[36,37] Absorption corrections were performed semi-empirically from equivalent reflections on basis of multi-scans (Bruker AXS APEX3). Hydrogen atoms were refined using a riding model or rigid methyl groups. In ***D***-1·***St***-1 in residue 3 the central CHCH unit is disordered over two positions. The ADPs of the atoms of the smaller component could only be refined isotropically. ***D***-2·***St***-3 was refined as a 2-component inversion twin. The central CHCH unit of residue 2 was disordered over two positions. ***D***-3·***St***-1 was also refined as a 2-component inversion twin. A solution in $P2_1/m$ is also possible but leads to severe disorder. Furthermore, the central CHCH unit of residue 3 is diordered over two position. The ADPs of the atoms of the smaller component could only be refined isotropically. The n-propyl group of residue 1 is disordered over two positions. The ADPs of both components could only be refined isotropically and SADI restraints were applied to the bond lengths. CCDC-1866420 (***D***-1·***St***-1), -1866422 (***D***-2·***St***-3) and -1866421 (***D***-3·***St***-1) contain the supplementary crystallographic data for this paper. These data can be obtained free of charge from The Cambridge Crystallographic Data Centre via www.ccdc.cam.ac.uk/data_request/cif.

Computational Analysis

The structures of all dimers and monomers were optimized with the TURBOMOLE V6.3 quantum chemistry program package[38] on the dispersion-corrected density functional (DFT+D) level of theory within C_s symmetry constraints. The reparametrized B97 functional[39] was employed in conjunction with a third-generation dispersion correction[40] and the def2-TZVP basis set.[41,42] The resolution-of-the-identity (RI) approximation was utilized with the appropriate auxiliary basis functions.[42] Interaction energies were obtained as energy differences without application of a counterpoise correction. The visualization of the electrostatic potential *Vs*(r) was created with the program MoleCoolQt[43] using the electron density values and electrostatic potential values computed for the monomers.

ASSOCIATED CONTENT

Supporting Information. Spectral data, thermal data. "This material is available free of charge via the Internet at http://pubs.acs.org."

AUTHOR INFORMATION

Corresponding Author

*michael.giese@uni-due.de
*arri.priimagi@tut.fi

Author Contributions

M. Sp. synthetized the molecules, M. Sa., M. Sp. and K. K. characterized the molecules, M. Sa., K. K., and M. V. performed the photochemical studies, M. P., G. J. and R. G. worked out the theoretical calculations, C. W. solved the crystal structures, M. G., A. P. and P. M. conceived and directed the project, M. Sa., M. G. and A. P. analyzed the data and wrote the paper. All the authors discussed the results and commented on the manuscript.

ACKNOWLEDGMENT

The research was generously supported by Professor Werdelmann foundation, Fonds der Chemischen Industrie and Mercator Research Center Ruhr. A.P. acknowledges the financial support of the Academy of Finland (Decision numbers 277091 and 312628) and the European Research Council (Starting Grant Project PHOTOTUNE, Decision number 679646).

REFERENCES

(1) Aida, T.; Meijer, E.; Stupp, S. Functional supramolecular polymers *Science* **2012**, *335*, 813– 817.

(2) Steed, J. W. Supramolecular Gel Chemistry: Developments over the Last Decade *Chem. Commun*. **2011**, *47*, 1379– 1383.

(3) a) Paleos, C. M.; Tsiourvas, D. Supramolecular Hydrogen-bonded Liquid Crystals *Liq. Cryst*. **2001**, *28*, 1127– 1161; b) Bisoyi, H. K.; Li, Q. Light-Driven Liquid Crystalline Materials: From Photo-Induced Phase Transitions and Property Modulations to Applications, *Chem. Rev*. **2016**, *116*, 15089– 15166.

(4) Desiraju, G. R.; Ho, P. S.; Kloo, L.; Legon, A. C.; Marquardt, R.; Metrangolo, P.; Politzer, P.; Resnati, G.; Rissanen, K. Definition of the Halogen Bond (IUPAC Recommendations 2013) *Pure Appl. Chem*. **2013**, *85*, 1711– 1713.

(5) a) Kolář, M. H.; Hobza, P. Computer Modeling of Halogen Bonds and Other σ-Hole Interactions *Chem. Rev*. **2016**, *116*, 5155– 5187; b) Politzer, P.; Murray, J. S.; Clark, T. Halogen Bonding: an Electrostatically-Driven Highly Directional Noncovalent Interaction *Phys. Chem. Chem. Phys*. **2010**, 12, 7748– 7757.

(6) a) Legon, A. C. Prereactive Complexes of Dihalogens XY with Lewis Bases B in the Gas Phase: A Systematic Case for the Halogen Analogue B···XY of the Hydrogen Bond B···HX *Angew. Chem., Int. Ed*. **1999**, *38*, 2686– 2714; b) Shields, Z. P.; Murray, J. S.; Politzer, P. Directional Tendencies of Halogen and Hydrogen Bonds *Int. J. Quantum Chem*. **2010**, *110*, 2823– 2832.

(7) Nguyen, H. L.; Horton, P. N.; Hursthouse, M. B.; Legon, A. C.; Bruce, D. W. Halogen Bonding: A New Interaction for Liquid Crystal Formation *J. Am. Chem. Soc*. **2004**, *126*, 16– 17

(8) Metrangolo, P.; Präsang, C.; Resnati, G.; Liantonio, R.; Whitwood, A. C.; Bruce, D. W. Fluorinated Liquid Crystals by Halogen Bonding *Chem. Commun*. **2006**, 3290– 3292.

(9) González, L.; Gimeno, N.; Tejedor, R. M.; Polo, V.; Ros, M. B.; Uriel, S.; Serrano, J. L. Halogen-Bonding Complexes Based on Bis(iodoethynyl)benzene Units: A New Versatile Route to Supramolecular Materials *Chem. Mater*. **2013**, *25*, 4503– 4510.

(10) McAllister, L. J.; Prasang, C.; Wong, J. P. W.; Thatcher, R. J.; Whitwood, A. C.; Donnio, B.; O'Brien, P.; Karadakov, P. B.; Bruce, D. W. Halogen-bonded liquid crystals of 4-alkoxystilbazoles with molecular iodine: a very short halogen bond and unusual mesophase stability *Chem. Commun*. **2013**, *49*, 3946– 3948.

(11) Yu, H.; Ikeda, T. Photocontrollable Liquid-Crystalline Actuators *Adv. Mater*. **2011**, *23*, 2149– 218.

(12) Mahimwalla, Z.; Yager, K. G.; Mamiya, J.; Shishido, A.; Priimagi, A.; Barrett, C. J. Azobenzene photomechanics: prospects and potential applications *Polym. Bull*. **2012**, *69*, 967– 1006.

(13) De Sio, L.; Tabiryan, N.; Bunning, T.; Kimball, B. R.; Umeton, C. Dynamic Photonic Materials Based on Liquid Crystals *Prog. Opt*. **2013**, *58*, 1– 64.

(14) Yagai, S.; Kitamura, A. Recent advances in photoresponsive supramolecular self-assemblies *Chem. Soc. Rev*. **2008**, *37*, 1520– 1529.

(15) Klajn, R. Immobilized azobenzenes for the construction of photoresponsive materials *Pure Appl. Chem*. **2010**, *82*, 2247– 2279.

(16) a) Bléger, D.; Schwarz, J.; Brouwer, A. M.; Hecht, S. o-Fluoroazobenzenes as Readily Synthesized Photoswitches Offering Nearly Quantitative Two-Way Isomerization with Visible Light *J. Am. Chem. Soc.* **2012**, *134*, 20597– 20600; b) Knie, M. Utecht, F. Zhao, H. Kulla, S. Kovalenko, A. M. Brouwer, P. Saalfrank, S. Hecht and D. Bléger, *Chem. Eur. J*., 2014, **20**, 16492–16501;

(17) a) Hird, M. Fluorinated Liquid Crystals – Properties and Applications *Chem. Soc. Rev*. **2007**, *36*, 2070– 2095; b) Tschierske, C. Fluorinated Liquid Crystals: Design of Soft Nanostructures and Increased Complexity of Self-Assembly by Perfluorinated Segments *Top. Curr. Chem*. **2011**, *318*, 1– 108.

(18) a) Fernandez-Palacio, F.; Poutanen, M.; Saccone, M.; Siiskonen, A.; Terraneo, G.; Resnati, G.; Ikkala, O.; Metrangolo, P.; Priimagi, A. *Chem. Mater*. **2016**, *28*, 8314– 8321; b) Saccone, M.; Palacio, F. F.; Cavallo, G.; Dichiarante, V.; Virkki, M.; Terraneo, G.; Priimagi, A.; Metrangolo, P. *Faraday Discuss*. **2017**, *203*, 407– 422.

(19) Priimagi, A.; Saccone, M.; Cavallo, G.; Shishido, A.; Pilati, T.; Metrangolo, P.; Resnati, G. Photoalignment and Surface-Relief-Grating Formation Are Efficiently Combined in Low-Molecular-Weight Halogen-Bonded Complexes *Adv. Mater*. **2012**, *24*, OP345– OP352.

(20) Chen, Y.; Yu, H.; Zhang, L.; Yang, H.; Lu, Y. Photoresponsive Liquid Crystals Based on Halogen Bonding of Azopyridines *Chem. Commun*. **2014**, *50*, 9647– 9649.

(21) Bushuyev, O. S.; Corkery, T. C.; Barrett, C. J.; Friscic, T. Photomechanical azobenzene cocrystals and in situ X-ray diffraction monitoring of their optically-induced crystal-to-crystal isomerisation *Chem. Sci*. **2014**, *5*, 3158– 3164.

(22) a) Saccone, M.; Cavallo, G.; Metrangolo, P.; Resnati, G.; Priimagi, A. Halogen-Bonded Photoresponsive Materials *Top. Curr. Chem*. **2014**, 359, 147– 166; b) Christopherson, J.-C.; Topić, F.; Barrett, C. J.; Friščić, T. Halogen-Bonded Cocrystals as Optical Materials: Next-Generation Control over Light–Matter Interactions. *Cryst. Growth Des.* **2018**, *18*, 1245– 1259.

(23) a) Valerio, G.; Raos, G.; Meille, S. V.; Metrangolo, P.; Resnati, G. Halogen Bonding in Fluoroalkylhalides: A Quantum Chemical Study of Increasing Fluorine Substitution *J. Phys. Chem. A* **2000**, *104*, 1617– 1620; b) Riley, K. E.; Murray, J. S.; Fanfrlík, J.; Řezáč, J.; Solá, R. J.; Concha, M. C.; Ramos, F. M.; Politzer, P. Halogen Bond Tunability I: The Effects of Aromatic Fluorine Substitution on the Strengths of Halogen-Bonding Interactions Involving Chlorine, Bromine, and Iodine *J. Mol. Model*. **2011**, *17*, 3309– 3318

(24) Ahmed, Z.; Siiskonen, A.; Virkki, M.; Priimagi, A. Controlling azobenzene photoswitching through combined *ortho*-fluorination and-amination *Chem. Commun*. **2017**, *53*, 12520– 12523.

(25) Alvarez, S. A cartography of the van der Waals territories *Dalton Trans*. **2013**, *42*, 8617– 8636.

(26) Saccone, M.; Terraneo, G.; Pilati, T.; Cavallo, G.; Priimagi, A.; Metrangolo, P.; Resnati, G. Azobenzene-based difunctional halogen-bond donor: towards the engineering of photoresponsive cocrystals *Acta Crystallogr*. **2014**, *B70*, 149–156.

(27) Jeffrey, G. A. An Introduction to Hydrogen Bonding; Oxford University Press: New York, **1997**; Vol. 12.

(28) a) D'Oria, E.; Novoa, J. J. The strength–length relationship at the light of ab initio computations: does it really hold? *CrystEngComm* **2004**, *6*, 368– 376; b) Gavezzotti, A. Computational studies of crystal structure and bonding *Top. Curr. Chem*. **2012**, *315*, 1– 32; c) Dunitz, J. D. Intermolecular atom–atom bonds in crystals? *IUCrJ* **2015**, *2*, 157– 158.

(29) Syz, M.; Zollinger, H. Die HAMMETT'sche Substituentenkonstanten fur m- und p-ständige Phenylazogruppen *Helv. Chim. Acta*, **1965**, *48*, 283– 385.

(29) Pfletscher, M.; Wölper, C.; Gutmann, J. S.; Mezger, M.; Giese, M. A modular approach towards functional supramolecular aggregates–subtle structural differences inducing liquid crystallinity *Chem. Commun*. **2016**, *52*, 8549– 8552

(31) Gray, G. W.; Hogg, C.; Lacey, D. The Synthesis and Liquid Crystal Properties of Some Laterally Fluorinated *trans*-Cyclohexane-1-carboxylate and Benzoate Esters *Mol. Cryst. Liq. Cryst*., **1981**, *67*, 1–23.

(32) Saccone, M.; Kuntze, K.; Ahmed, Z.; Siiskonen, A.; Giese, M.; Priimagi, A.; *Ortho*-fluorination of azophenols increases the mesophase stability of photoresponsive hydrogen-bonded liquid crystals *J. Mater. Chem. C*, **2018**, *6*, 9958–9963.

(33) a) Tong, X.; Wang, G.; Zhao, Y. Photochemical Phase Transition Versus Photochemical Phase Separation *J. Am. Chem. Soc.* **2006**, *128*, 8746– 8747; b) Tong, X.; Zhao, Y. Multiple Photochemical Processes in Liquid Crystalline Azo Dye-Doped Liquid Crystals *Chem. Mater*. **2009**, *21*, 4047– 4054.

(34) a) Aakeröy, C. B.; Baldrighi, M.; Desper, J.; Metrangolo, P.; Resnati, G. Supramolecular Hierarchy among Halogen-Bond Donors *Chem. Eur. J*. **2013**, *19* (48), 16240– 16247; b) Saccone, M.; Dichiarante, V.; Forni, A.; Goulet-Hanssens, A.; Cavallo, G.; Vapaavuori, J.; Terraneo, G.; Barrett, C. J.; Resnati, G.; Metrangolo, P.; Priimagi, A. Supramolecular Hierarchy among Halogen and Hydrogen Bond Donors in Light-Induced Surface Patterning *J. Mater. Chem. C* **2015**, *3*, 759– 768.

(35) Sheldrick, G. M. Phase annealing in SHELX-90: direct methods for larger structures *Acta Crystallogr*. **1990**, *A46*, 467–473.

(36) Sheldrick, G. M. SHELXL-2014, Program for the Refinement of Crystal Structures University of Göttingen, Göttingen (Germany) **2014**.

(37) Hübschle, C. B.; Sheldrick, G. M.; Dittrich, B. shelXle, *A Qt GUI for SHELXL*, *J. Appl. Cryst.* **2011**, *44*, 1281–1284.

(38) TURBOMOLE V6.3 2011, a development of University of Karlsruhe and Forschungszentrum Karlsruhe GmbH, 1989-2007, TURBOMOLE GmbH, since 2007; available from http://www.turbomole.com.

(39) Grimme, S. Semiempirical GGA-type Density Functional Constructed with a Long-Range Dispersion Correction *J. Comput. Chem*. **2006**, 27, 1787– 1799.

(40) Grimme, S.; Antony, J.; Ehrlich, S.; Krieg, H. A Consistent and Accurate ab initio Parametrization of Density Functional Dispersion Correction (DFT-D) for the 94 Elements H-Pu *J. Chem. Phys.* **2010**, 132, 154104– 154119.

(41) Weigend, F.; Häser, M.; Patzelt, H.; Ahlrichs, R. RI-MP2: optimized auxiliary basis sets and demonstration of efficiency *Chem. Phys. Lett.* **1998**, 294, 143– 152.

(42) Eichkorn, K.; Weigend, F.; Treutler, O.; Ahlrichs, R. Auxiliary basis sets for main row atoms and transition metals and their use to approximate Coulomb potentials *Theor. Chem. Acc*. **1997**, 97, 119– 124.

(43) Hübschle, C. B.; Dittrich, B. MoleCoolQt - a molecule viewer for charge-density research *J. Appl. Crystallogr*. **2011**, 44, 238– 240.